JMEPEG (2014) 23:39–48
DOI: 10.1007/s11665-013-0749-y

©ASM International
1059-9495/$19.00

3D Numerical Simulation on Thermal Flow Coupling Field of Stainless Steel During Twin-Roll Casting

Lianlian Liu, Bo Liao, Jing Guo, Ligang Liu, Hongyan Hu, Yue Zhang, and Qingxiang Yang

(Submitted May 24, 2013; in revised form August 20, 2013; published online October 23, 2013)

The surface crack and lateral crack of the AISI 304 stainless steel thin strip produced by twin-roll casting were observed. The temperature at the center of outlet during twin-roll-casting process was determined by infrared thermometer. In order to avoid the surface cracks of the casting strip, the thermal flow coupling field of AISI 304 stainless steel during twin-roll-casting process was simulated by a 3D fluid-structure coupling model. According to the simulation result, the effect of the casting speed on thermal flow field was analyzed and the process parameters were optimized. Moreover, by studying heat flux curves, the heat transfer mechanism between molten pool and roll was analyzed. The results show that, with the increase of the casting speed, the temperature of the molten pool increases and the solidification point moves toward the outlet. Meanwhile, the whirlpool above gets larger. Based on the solidification front position, the optimized process parameters are 1500 °C and 0.37 m/s. The heat transfer mechanism between molten pool and roll contains direct contacting heat transfer and air gap heat transfer.

Keywords 3D fluid-structure coupling model, heat transfer mechanism, process parameters optimization, thermal flow coupling field, twin-roll casting

1. Introduction

In recent years, twin-roll-casting technology, has been developed to produce stainless steel thin strip whose thickness is 2-6 mm (Ref 1-3). Compared with traditional stainless steel production process, twin-roll-casting process can save about 70 % equipment cost and 30-40 % production investment (Ref 4). Moreover, solidified microstructure refinement, micro-segregation reducement and solubility limit expansion can be obtained by twin-roll-casting process (Ref 5).

However, surface cracks often initiate in the strip produced by twin-roll casting (Ref 6, 7), which is closely related to the casting speed (Ref 8). If the casting speed is too low, the liquid steel will solidify long before it reaches the outlet, so the strip may fracture because of large stress from roll at the outlet. While, if the casting speed is too high, the liquid steel will not solidify until it reaches the outlet, so the strip may also fracture because of the too low allowable stress. Therefore, it is necessary to control the solidification point by adjusting the casting speed.

During the actual production, the controllable range of the casting speed is very narrow. It is difficult to investigate the process by experiment. Therefore, many researchers have concentrated on the simulation of flow and temperature fields. Santos et al. (Ref 9) developed a 2D solidification model and simulated the solidification process of the casting strip. Kim et al. (Ref 10) proposed a 2D-coupled turbulent flow and heat transfer model of wedge-shaped pool and investigated the effects of nozzle type on the flow and temperature fields. Miao et al. (Ref 11) underlined the importance of the axial flow and proposed a 3D model to simulate the flow, heat transfer, and solidification during twin-roll casting. Zhang et al. (Ref 12) used a 3D model to give the effects of the pouring temperature and the height of liquid level on the flow and temperature fields. They adopted vary heat transfer coefficients at different contacting regions between molten pool and roll and simulated the heat transfer more accurately. However, all of these researchers only modeled the molten pool and discarded the roll. The heat transfer style between molten pool and roll was simplified as convection type, which can only considered the radial direction heat transfer. During actual production, only a small part of heat was transferred along radial direction of the roll. The heat was mainly transferred along the circumfluent direction of the roll (Ref 13). To solve this problem, a 3D fluid-structure coupling model was proposed in this work. By adopting different casting speeds, the effects of the casting speed on thermal flow field were analyzed and the casting speed was optimized. Moreover, by studying heat flux curves, the heat transfer mechanism between molten pool and roll was analyzed.

2. Experimental Materials and Methods

During the twin-roll casting, the two rolls rotate in the opposite direction with the same speed. The liquid steel offered by the casting system is accepted by rotating roll and transports to the outlet. Because of the rolling force from roll and the cooling effect from roll and side dams, the casting strip is obtained at the outlet. The schematic chart of the twin-roll-casting process is shown in Fig. 1.

Lianlian Liu, Bo Liao, Jing Guo, Ligang Liu, Hongyan Hu, and **Qingxiang Yang**, State Key Laboratory of Metastable Materials Science & Technology, Yanshan University, Qinhuangdao 066004, People's Republic of China; and **Yue Zhang**, College of Materials Science and Engineering, University of Science and Technology, Beijing 100083, People's Republic of China. Contact e-mail: qxyang@ysu.edu.cn.

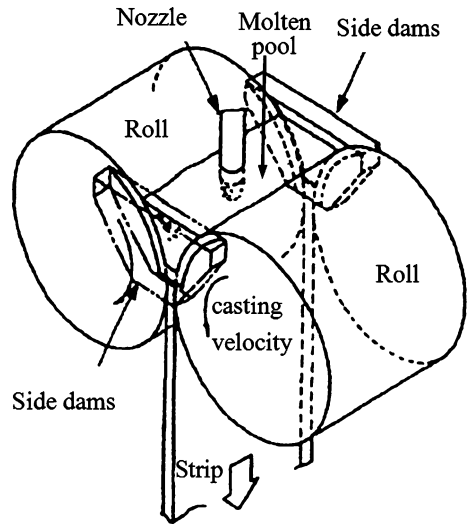

Fig. 1 Schematic chart of the twin-roll-casting process

In the actual production of AISI 304 stainless steel, whose composition is listed in Table 1, the temperature at the center of outlet is determined by infrared thermometer. The cracking specimen was taken from the thin strip produced by twin-roll-casting process, which is shown in Fig. 2 and the surface cracks and lateral cracks were observed by Axiovert 200 MAT optical microscope (OM) after corroded by aqua regia (HNO_3 + 3HCl).

3. Mathematical Model

3.1 Governing Equations

The geometry of the computational domain is shown in Fig. 3, in which the origin of the coordinate system is at the center of the symmetry. During the twin-roll casting, the state of the molten pool is very complex because the solid region, liquid region, and liquid-solid region exist synchronously. Therefore, the generalized liquid method (Ref 13) is adopted. Considering the flow characteristics during twin-roll casting, the K-ε model (Ref 14) is used. The governing equations are as follows:

The continuity equation:

$$\frac{\partial \rho}{\partial t} + \nabla \cdot (\rho v) = 0. \quad \text{(Eq 1)}$$

The momentum equation:

$$\rho\left[\frac{\partial v}{\partial t} + (v \cdot \nabla)v\right] = -\nabla p + \bar{F} - \nabla \times [\mu(\nabla \times v)] + \nabla[(\lambda + 2\mu)\nabla \times v]. \quad \text{(Eq 2)}$$

The energy equation:

$$\rho\frac{DH}{Dt} = \frac{D\rho}{Dt} + \frac{\partial q_v}{\partial t} + \Phi + \nabla \cdot (k\nabla T) - \nabla \cdot \bar{q}_r \quad \text{(Eq 3)}$$

where v is velocity, μ is dynamic viscosity, λ is viscosity coefficient, p is pressure, $\bar{F}$ is physical force of unit volume, H is enthalpy of unit mass, q_v is heat generation rate of unit volume, Φ is mechanical or viscous dissipation coefficient, and $\bar{q}_r$ is radiation heat flux.

Table 1 Composition of AISI 304 stainless steel (weight percent)

C	Cr	Ni	Mn	Si	Mo	Fe
0.06	18	8	1.2	0.7	0.18	Bal.

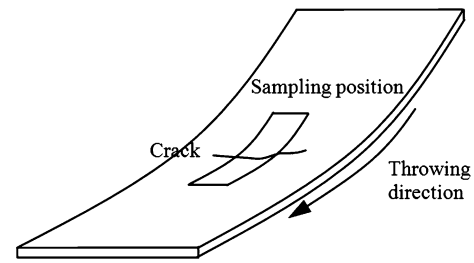

Fig. 2 Schematic diagram of cracking specimen

3.2 Latent Heat of Solidification

Due to the difference of internal energy between different phases, the latent heat is released during the phase change, which can affect the temperature distribution. In this paper, the effective-specific heat method is adopted to take latent heat of solidification into account. The specific heat can be expressed as follows:

$$c_{\text{pe}} = c_p - L\frac{\partial f_s}{\partial T} \quad \text{(Eq 4)}$$

where c_p is specific heat at constant pressure, c_{pe} is equivalent-specific heat at constant pressure, and f_s is fraction of solid phase in two-phase region.

The system (1-4) presents a general description of the physical phenomena that take part in the casting process considered. A particular application to the twin-roll casting is realized by ANSYS commercial software product.

3.3 Boundary Condition and Initial Condition

$$\text{On the inlet,} \quad v_x = v_z = 0,\ v_y = v_{\text{in}},\ k = av_{\text{in}}^2,\ \varepsilon = \frac{k^{1.5}}{R},\ T_{t=0} = T_0 \quad \text{(Eq 5)}$$

where v_x v_y and v_z are, respectively, velocity components in x, y, z direction; v_{in} is velocity into the inlet, k is turbulent kinetic energy, ε is turbulent eddy dissipation, a is experimentally determined parameter, R is hydraulics nozzle size and is temperature into the inlet.

$$\text{On the opening,} \quad v_y = 0,\ \frac{\partial v_x}{\partial y} = \frac{\partial v_z}{\partial y} = \frac{\partial k}{\partial y} = \frac{\partial \varepsilon}{\partial y} = 0,\ T_{t=0} = T_0 \quad \text{(Eq 6)}$$

$$\text{On the outlet,} \quad v_y = v,\ v_x = v_z = 0 \quad \text{(Eq 7)}$$

$$\text{On the central symmetry,} \quad v_z = 0,\ \frac{\partial v_x}{\partial y} = \frac{\partial v_y}{\partial y} = \frac{\partial k}{\partial y} = \frac{\partial \varepsilon}{\partial y} = 0 \quad \text{(Eq 8)}$$

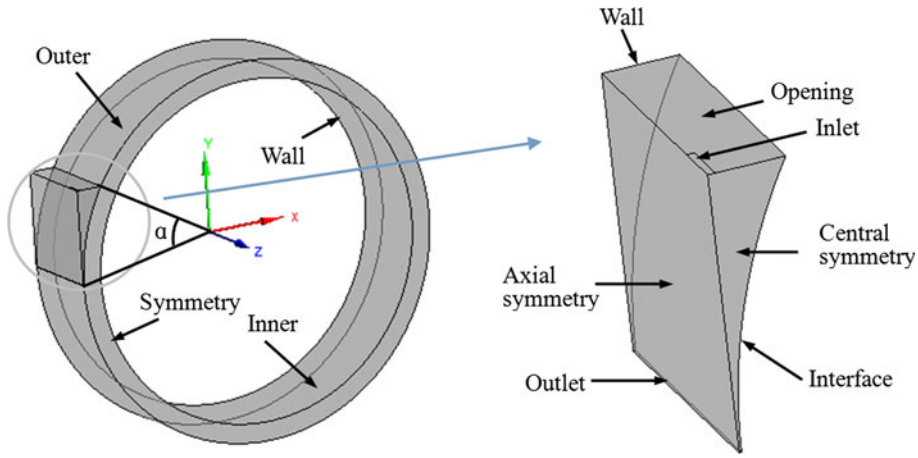

Fig. 3 Geometry of the computational domain

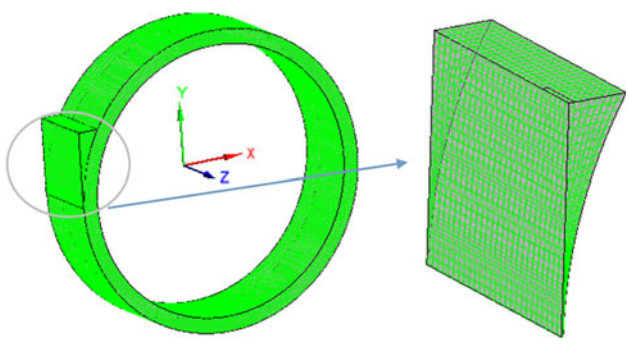

Fig. 4 Finite element model

On the axial symmetry, $v_x = 0,\ \frac{\partial v_z}{\partial y} = \frac{\partial v_y}{\partial y} = \frac{\partial k}{\partial y} = \frac{\partial \varepsilon}{\partial y} = 0$ (Eq 9)

On the interface, $v_x = -v\sin\theta,\ v_y = -v\cos\theta,\ v_z = 0$ (Eq 10)

where v is linear velocity of the roll and θ is contacting angle.

The heat transfer is calculated according to the fluid-structure coupling heat transfer model in CFX. The conservative interface flux is adopted.

On the wall, $v_z = 0,\ -\mathrm{k}\frac{\partial T}{\partial n} = h_\mathrm{c}(T - T_\mathrm{c})$ (Eq 11)

where h_c is heat transfer coefficient, T_c is the temperature of side dams, and it is regarded as constant at 1000 °C in this paper due to the excellent adiabatic property of side dams.

On the inner plane, $-k\frac{\partial T}{\partial n} = h_\mathrm{w}(T - T_\mathrm{w})$ (Eq 12)

where h_w is heat transfer coefficient between the roll and cooling water; T_w is the temperature of the cooling water.

Table 2 Process parameters for casting

Parameter	Value
Roll diameter, m^{-1}	0.5
Roll width, m^{-1}	0.25
Thin strip thickness, m^{-1}	0.002
Contact angle, α/°	30
Pouring temperature, °C	1500
Casting speed, $\mathrm{m}^{-1}\ \mathrm{s}^{-1}$	0.1, 0.2, 0.4

On the outer plane, only heat transfer is calculated and the conservative interface flux is adopted.

On the wall contacting with air, $-k\frac{\partial T}{\partial n} = h_\mathrm{air}(T - T_\mathrm{air})$ (Eq 13)

where h_air is heat transfer coefficient between the roll and air around, T_air is the temperature of the air.

On the symmetry, $\frac{\partial(\rho \mathrm{h})}{\partial t} = \nabla\cdot(\lambda\nabla T) + S_\mathrm{E} - \nabla\cdot(\rho U_\mathrm{S} h) = 0$ (Eq 14)

where h is entropy, S_E is volume heat source, and U_S is velocity.

3.4 Finite element model and process parameters

Considering the symmetry, a quarter of the real geometry is taken. By ICEM module, the hexahedral grid is divided, which is shown in Fig. 4. The model contains 54912 elements with 66528 nodes, corresponding to which, the molten pool model contains 5616 elements with 6804 nodes.

The process parameters are listed in Table 2, in which the contact angle is the central angle of the interface in the molten pool as shown in Fig. 3. The physical parameters adopted are listed in Table 3.

Table 3 Physical parameters of AISI 304 stainless steel

Density, kg m^{-3}	Molar mass, g mol^{-1}	Specific heat, J kg^{-1} °C^{-1}	Dynamic viscosity, Kg m^{-1} s^{-1}	Thermal conductivity, W m^{-1} K^{-1}
7060	55.2	809.27	0.00685	33.51

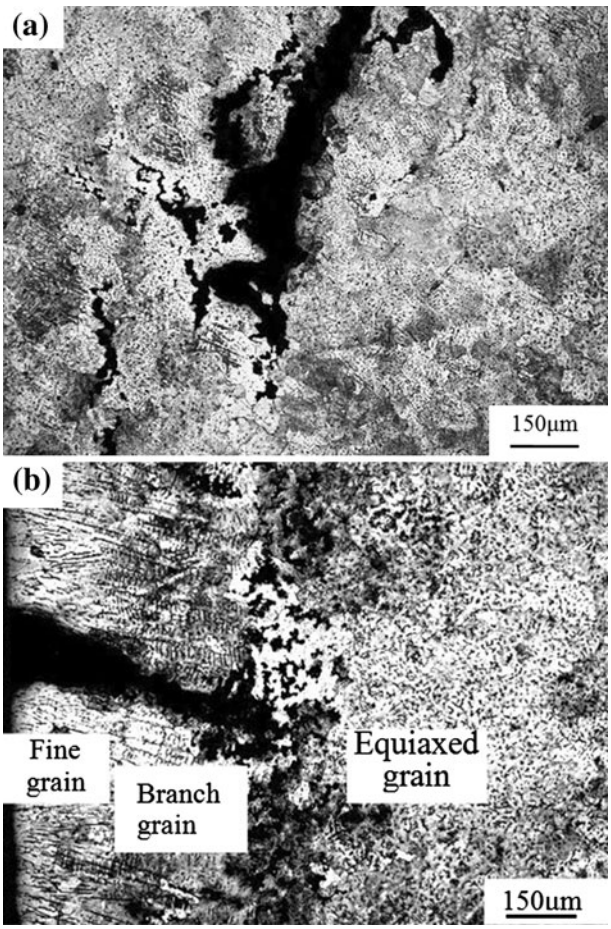

Fig. 5 Surface and lateral cracks of casting strip: (a) surface cracks and (b) lateral cracks

The physical parameters needed for simulating are provided by Jmatpro software. The software is excellent in providing physical property parameters for a lot of simulation software, such as Procast, Anycasting, Dvnaform, Deform, and so on.

4. Experimental results and analysis

4.1 Surface and Lateral Cracks of Casting Strip

The surface cracks of the casting strip are shown in Fig. 5(a). It can be seen that large intergranular cracks exist in the casting strip surface. The width of cracks reaches 100 μm and the cracks propagate circuitously.

The lateral cracks of casting strip are shown in Fig. 5(b). It indicates that, from surface to center, the microstructures are fine grain, branch grain, and equiaxed grain microstructures, respectively. The cracks initiate from the surface, propagate inward and terminate in the interface between branch grain zone and equiaxed grain zone.

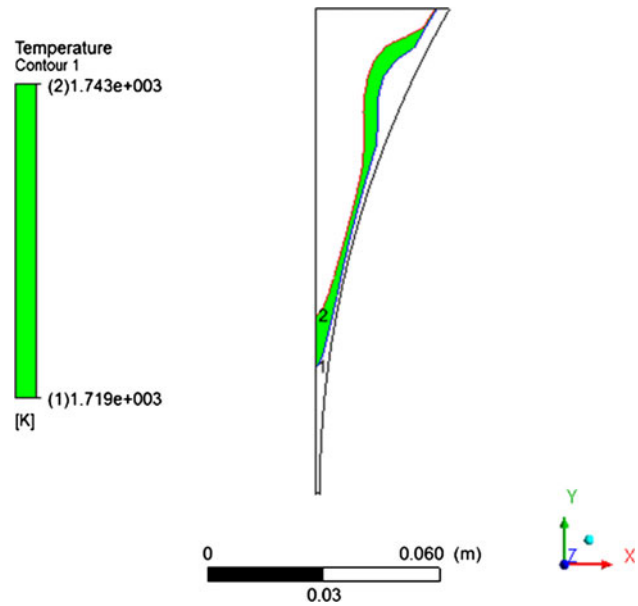

Fig. 6 Solidification front position

4.2 Temperature at the Center of Outlet

In production of AISI 304 stainless steel, the process parameters were 1500 °C, 0.1 m/s. The temperature at the center of outlet determined is about 1370 °C.

5. Simulation Results and Analysis

5.1 Temperature at the Center of Outlet

When the process parameters are 1500 °C and 0.1 m/s, the temperature at the center of outlet obtained by simulation is 1363 °C, which is in accordance with the determined result. Therefore, the model used in this work is effective, which can be used for subsequent simulation.

5.2 Solidification Front Position

The isoline of solidification point (1719 K), is shown in Fig. 6, when the process parameters are 1500 °C and 0.1 m/s. It can be seen that the thin strip has solidified long before it reaches the outlet, which can lead to large rolling force at the outlet. When the stress exceeds the allowable stress of the steel,

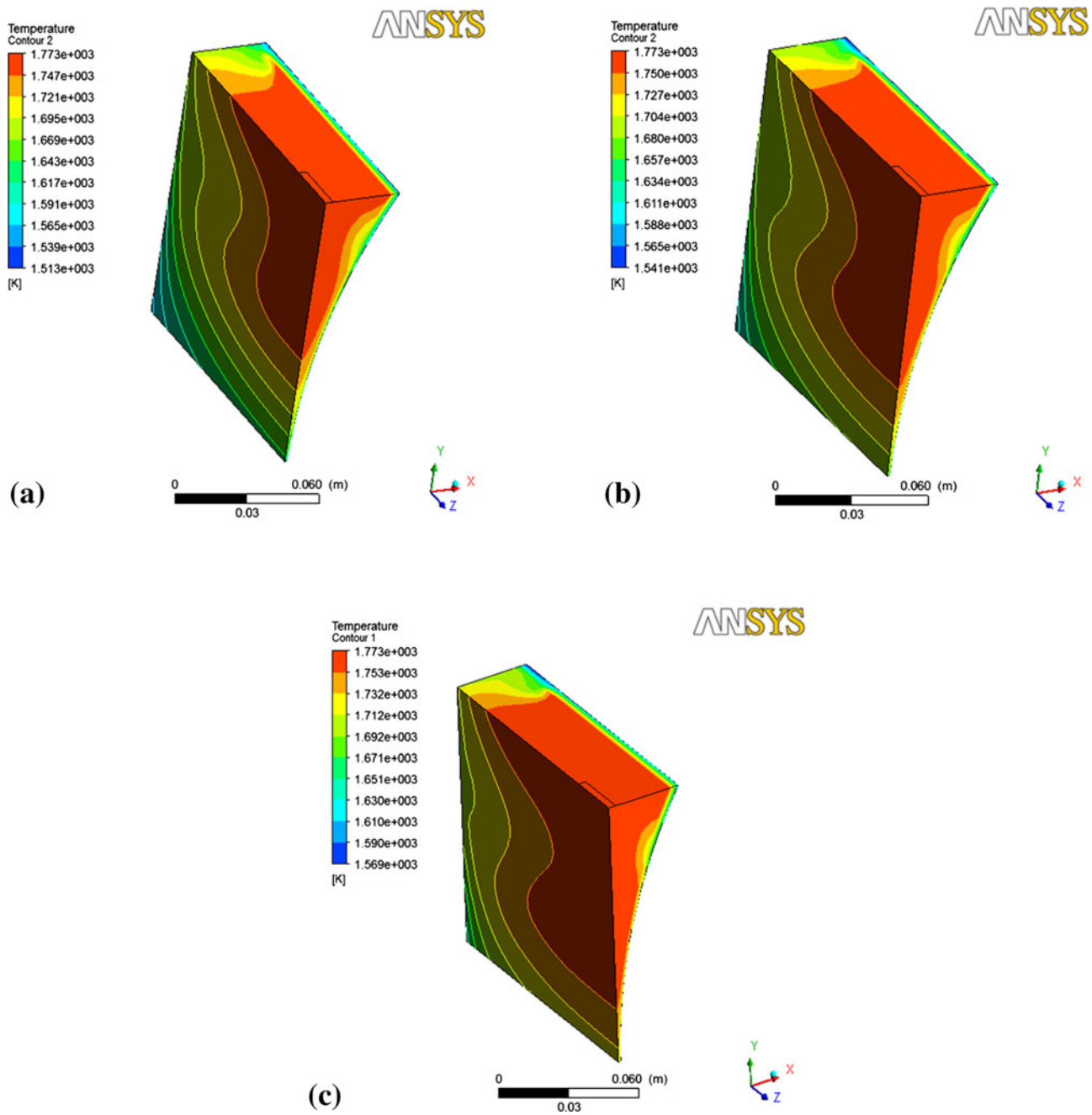

Fig. 7 Temperature distribution of molten pool: (a) 0.1 m/s, (b) 0.2 m/s, and (c) 0.4 m/s

the cracks initiate, which accounts for the crack of thin strip as shown in Fig. 5.

5.3 Effects of Casting Speed on Thermal Flow Coupling Field

The temperature distribution is an important factor that affects the microstructure and quality of the casting strip. So Figs. 7 and 8 give the temperature distributions of the molten pool and roll with different casting speeds.

From Fig. 7, the temperature near the inlet is higher. While, the temperature near the interface and the outlet is lower. The thin shell of the stainless steel can form as soon as it contacts the interface and the strip can be obtained at the outlet. The temperature near the whirlpools is 30-80 °C lower than the around region because of the reflux of molten steel.

Figure 7 also shows, with the casting speed increasing, the temperature of the molten pool increases. The reason is that the faster the casting speed is, the shorter the time that molten steel contacts with the roll is, so the less the energy transferred from molten pool to the pool is.

From Fig. 8, the temperature near the contact region with the molten pool is higher, which indicates the heat is well transferred to the roll from the molten pool. While, it also

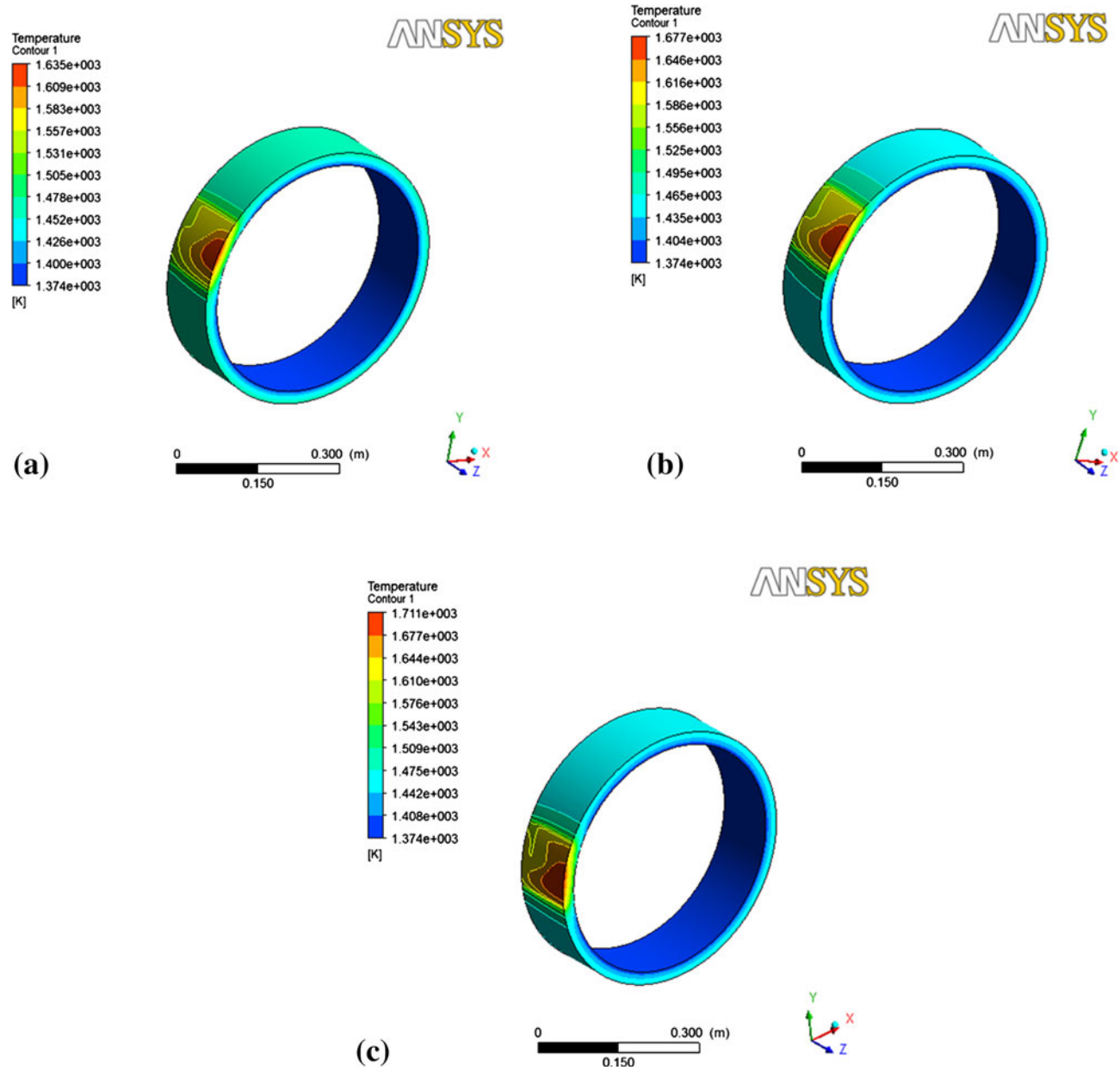

Fig. 8 Temperature distribution of roll: (a) 0.1 m/s, (b) 0.2 m/s, and (c) 0.4 m/s

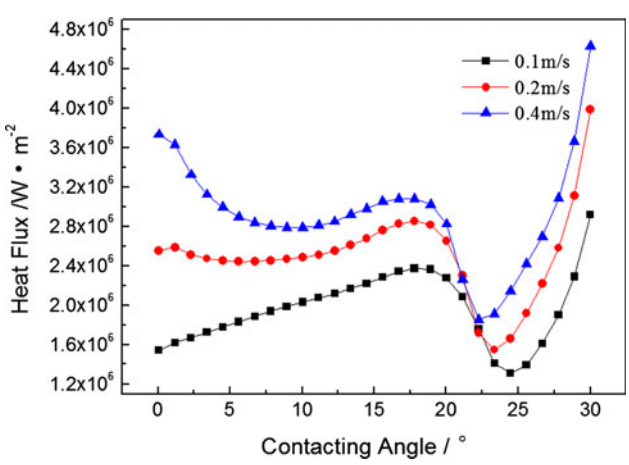

Fig. 9 Heat flux vs. contacting angle with different casting speeds

indicates that the roll will suffer sever thermal cycle and the improvement of the fatigue life is of great importance.

Figure 9 shows the heat flux curves. It indicates that the faster the casting speed is, the larger the heat flux between the molten pool and the roll is.

When the casting speed is large, the molten pool and roll can not contact sufficiently, so temperature gradient between molten pool and roll is large and the heat flux is large, too.

Moreover, the three curves are similar to each other. The heat flux is large when the solidified shell contacts with the roll closely. The heat transfer style in this stage is direct contacting heat transfer. With the decrease of contacting angle, solidification shrinkage leads to the partial separation between the solidified shell and the roll, so the heat flux decreases. The heat transfer style in this stage is air gap heat transfer. With the further decrease of contacting angle, affected by extrusion of roll, the solidified shell can once

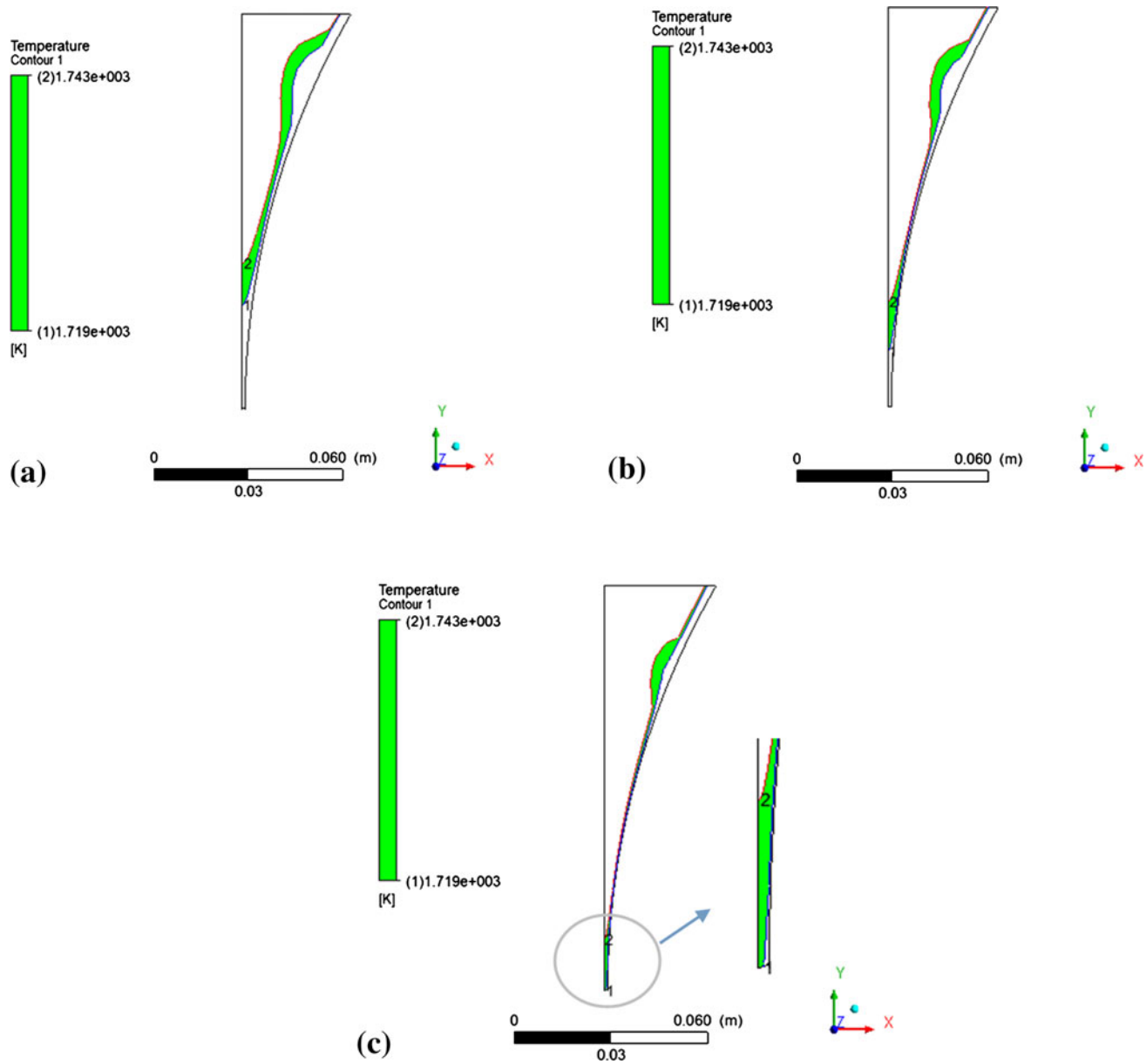

Fig. 10 Solidification front position: (a) 0.1 m/s, (b) 0.2 m/s, and (c) 0.4 m/s

again contact closely with the roll, so the heat flux increases again and reaches its peak at about 17°. When the contacting angle is lower that 17°, the temperature of the solidified shell is already relatively low, which lead to the low temperature gradient between the solidified shell and roll, so the heat flux is low, too.

The effect of the casting speed on solidification point is shown in Fig. 10. It can be seen that the solidification point moves toward the outlet with the increase of the casting speed.

When the casting speed is lower than 0.2 m/s, the thin strip has solidified long before it reaches the outlet, which may lead to strip crack because of the large stress at the outlet. While, when the casting speed is higher than 0.4 m/s, the thin strip has not solidified fully until it reaches the outlet, which may also lead to strip crack because of low allowable stress. Therefore, to obtain strip with good quality, the appropriate casting speed is between 0.2 and 0.4 m/s.

Figures 11 and 12 show the flow field distributions in central symmetry and axial symmetry, respectively. It indicates that for casting speed from 0.1 to 0.4 m/s, two whirlpools exist in the molten pool. In the upper of the molten pool, due to the higher temperature, the viscosity is smaller. Eroded by the liquid steel, the above whirlpool forms. As the molten steel flows toward the outlet, the temperature decreases and the viscosity increases. However,

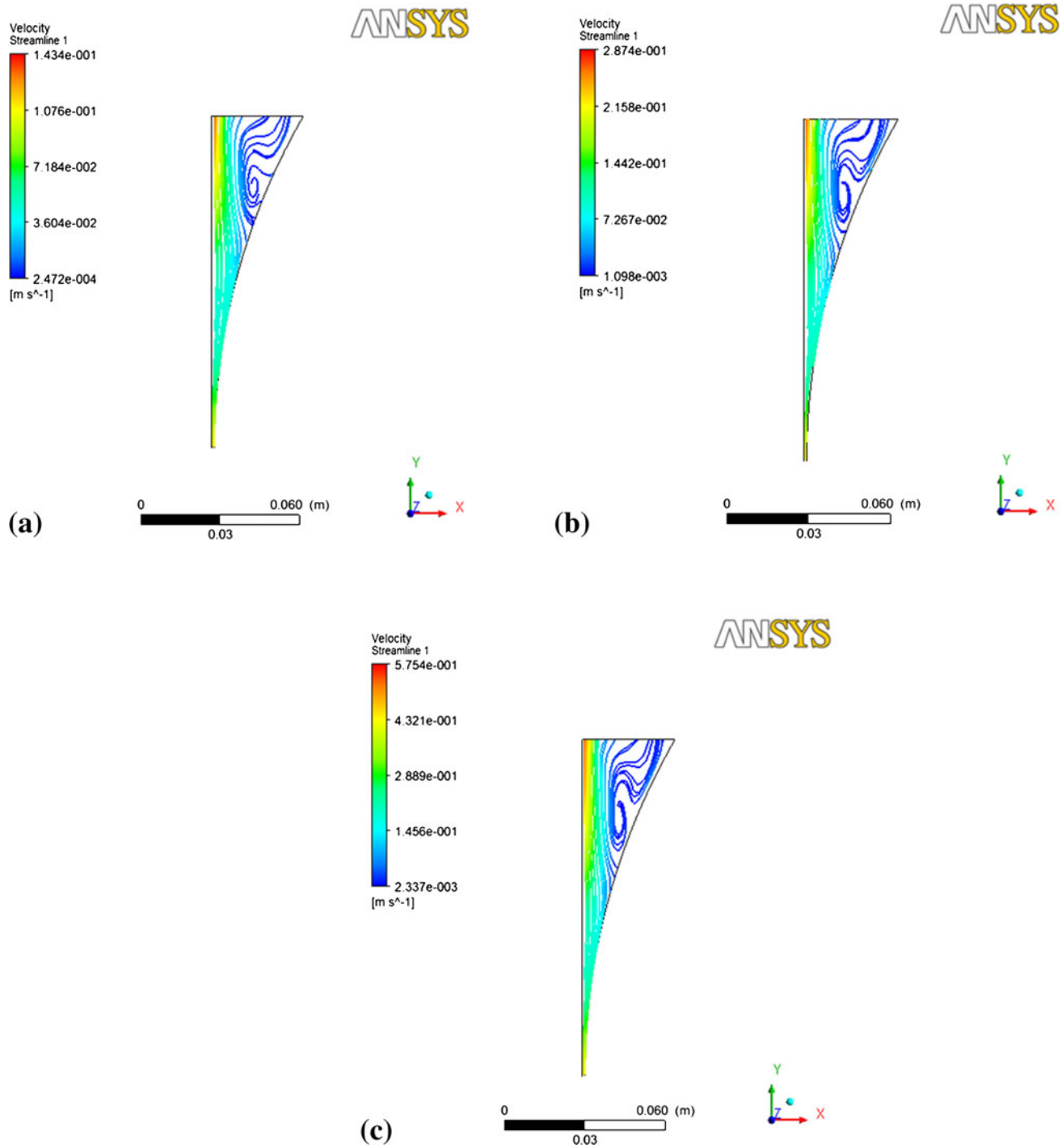

Fig. 11 Flow field distribution of central symmetry: (a) 0.1 m/s, (b) 0.2 m/s, and (c) 0.4 m/s

because of the rotating of roll, the other whirlpool forms. The existence of the whirlpools is beneficial to the temperature and composition homogeneousness.

Figures 11 and 12 also show, with the increase of casting speed, the upper whirlpool gets larger. The reason is that the faster the casting speed is, the more obvious the liquid steel erosion gets.

5.4 Process Parameters Optimization

If the solidification point is too high, the liquid steel will solidify long before it reaches the outlet, so the strip may fracture because of large stress from roll at the outlet. While, if the solidification point is too low, the liquid steel will not solidify until it reaches the outlet, so the strip may also fracture

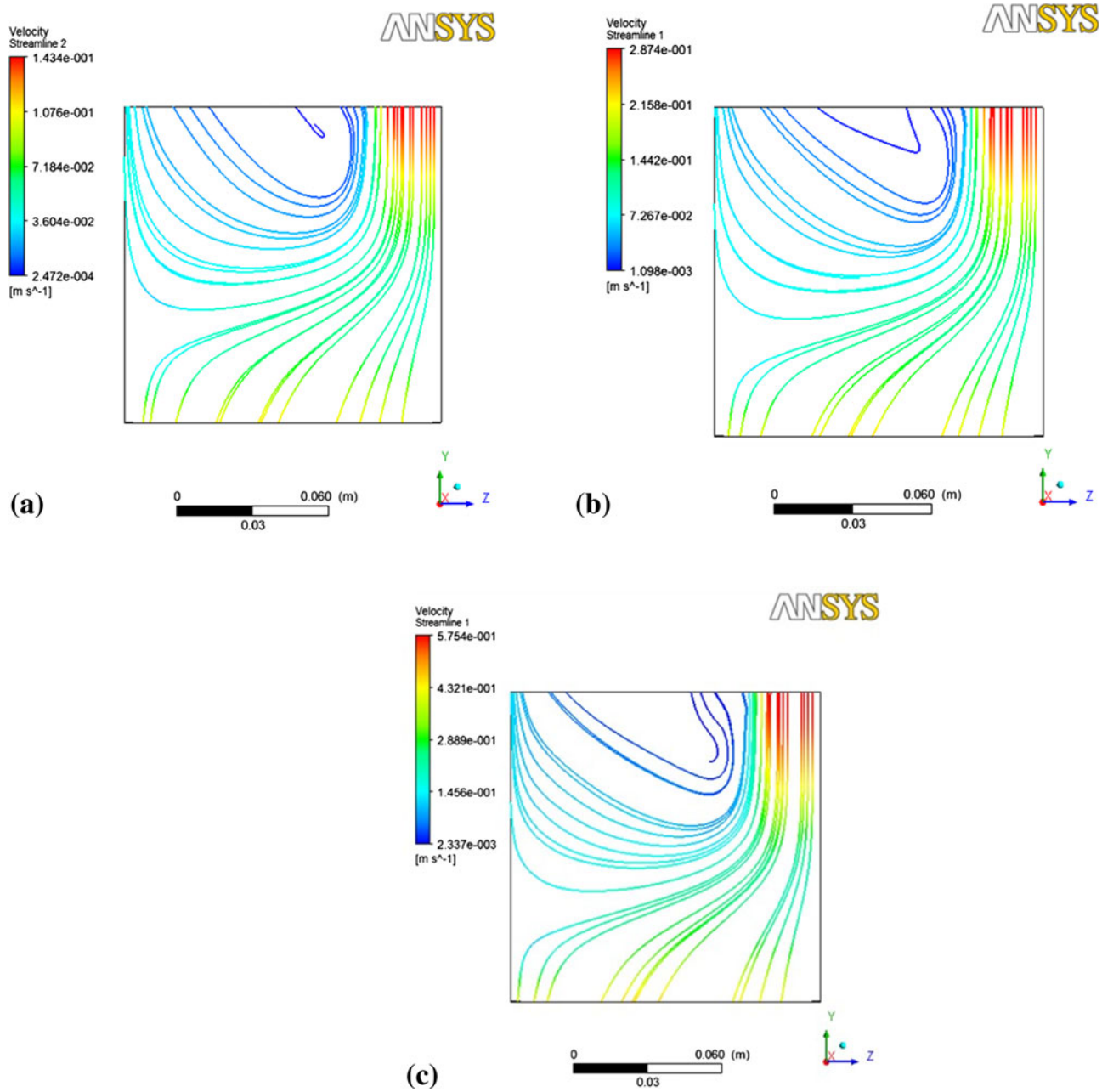

Fig. 12 Flow field distribution of axial symmetry: (a) 0.1 m/s, (b) 0.2 m/s, and (c) 0.4 m/s

because of the too low allowable stress. Based on this theory, the process parameters are optimized.

Figure 13 shows the temperature distribution at central symmetry line (intersection of central symmetry and axial symmetry) with different casting speeds.

By fitting the temperature at the outlet with the casting speed, the optimized casting speed that can make the solidification point just at the outlet is obtained, which is 0.37 m/s.

Using the optimized casting speed (0.37 m/s), the thermal and flow coupling field was simulated. The solidification front position obtained is shown in Fig. 14. It can be seen that the liquid steel solidifies fully just at the outlet, which proves the correctness of the optimization.

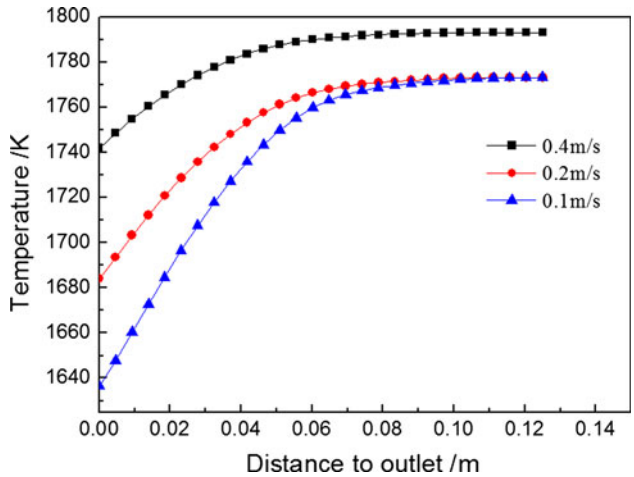

Fig. 13 Temperature distribution at central symmetry line

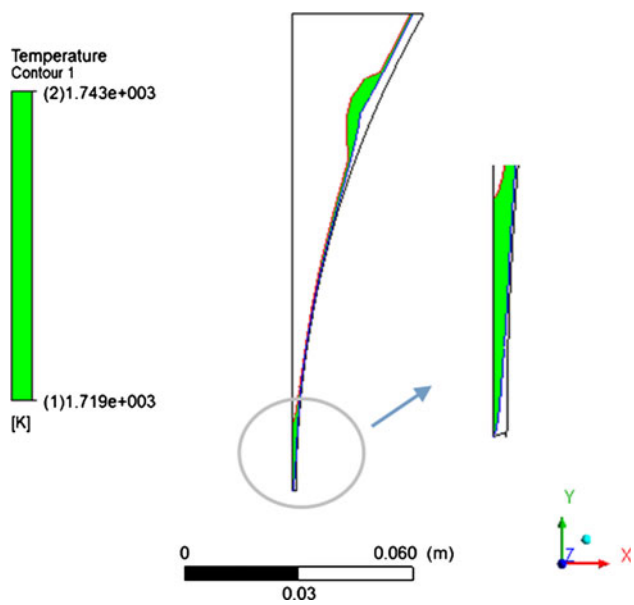

Fig. 14 Solidification front position with 1500 °C, 0.37 m/s

6. Conclusions

(1) On the casting strip surface, the cracks are intergranular cracks and their width reaches 100 μm. The cracks initiate from the surface, propagate inward, and terminate in the interface between branch grain zone and equiaxed grain zone. From surface to center, the microstructures are fine grain, branch grain, and equiaxed grain microstructures, respectively.

(2) The simulated result is in accordance with the determined one, which indicates the model established in this work is effective. Simulation results show that, with the increase of the casting speed, the temperature of the molten pool increases and the solidification point moves toward the outlet. Meanwhile, the whirlpool above gets larger and the heat transfer between molten pool and the roll increases.

(3) The heat transfer mechanism between molten pool and the roll contains direct contacting heat transfer and air gap heat transfer.

(4) On the basis of the solidification front position, the optimized process parameters are obtained, which are 1500 °C and 0.37 m/s.

Acknowledgements

The authors would like to express their gratitude for projects supported by the Natural Science Foundation (E2012203019) of Hebei Province of China.

References

1. Y.J. Park and H.S. Cho, A Fuzzy Logic Controller for the Molten Steel Level Control of Strip Casting Processes, *Control Eng. Pract.*, 2005, **7**(13), p 821 [in English]
2. C.M. Park, W.S. Kim, and G.J. Park, Thermal Analysis of the Roll in the Strip Casting Process, *Mech. Res. Commun.*, 2003, **4**(30), p 297 [in English]
3. K.M. Mchugh, J.-P. Delplanque, S.B. Johnson, E.J. Lavernia, Y. Zhou, and Y. Lin, Spray Rolling Aluminum Alloy Strip, *Mater. Sci. Eng. A*, 2004, **1**(383), p 96 [in English]
4. Z. Nikolai, Comparison of Continuous Strip Casting with Conventional Technology, *ISIJ Int.*, 2003, **8**(43), p 1115–1127 [in English]
5. D.K. Choo, H.K. Moon, T. Kang, and S. Lee, Analysis and Prevention of Cracking during Strip Casting of AISI, 304 Stainless Steel, *Metall. Mater. Trans. A*, 2001, **9**(32), p 2249–2258 [in English]
6. Y. Hiroyu, T. Kazuyuki, K. Masahiko, and I. Takeshi, Surface Quality of Stainless Steel Type 304 Cast by Twin-roll Type Strip Caster, *ISIJ Int.*, 1995, **35**(6), p 784–789 [in English]
7. M. Ha, J. Choi, S. Jeong, H. Moon, T. Kang, and S. Lee, Analysis and Prevention of Microcracking Phenomenon Occurring during Strip Casting of an AISI, 304 Stainless Steel, *Metall. Mater. Trans. A*, 2002, **5**(33), p 1487–1497 [in English]
8. G.M. Cao, C.G. Li, Z.Y. Liu, D. Wu, G.D. Wang, and X.H. Liu, Numerical Simulation of Temperature Field Coupled with Flow Field during Twin-roll Strip Casting Process, *J. Iron Steel Res.*, 2008, **9**(20), p 23–27 [in Chinese]
9. C.A. Santos, J.A. Spim, and A. Garcia, Modeling of Solidification in Twin-roll Strip Casting, *J. Mater. Proc. Technol.*, 2000, **102**, p 33–39 [in English]
10. W.S. Kim, D.S. Kim, and A.V. Kuznetsov, Simulation of Coupled Turbulent Flow and Heat Transfer in the Wedged-shaped Pool of a Twin-roll Strip Casting Process, *Int. J. Heat Mass Transf.*, 2000, **43**, p 3811–3822 [in English]
11. Y.C. Miao, H.C. Di, X.M. Zhang, G.D. Wang, and X.H. Liu, Three - dimensional Simulation on the Twin Roll Casting Process of Stainless Strip, *Acta Metall. Sin.*, 2000, **10**(36), p 1109–1112 [in Chinese]
12. X.M. Zhang, Z.Y. Jiang, L.M. Yang, X.H. Liu, G.D. Wang, and A.K. Tieu, Modeling of Coupling Flow and Temperature Fields in molten Pool during Twin-roll Strip Casting Process, *J. Mater. Process. Technol.*, 2007, **187-188**, p 339–343 [in English]
13. Z.M. Jin, J.C. He, and G.X. Xu, Numerical Simulation on Flow, Temperature and Thermal Stress Fields during Twin Roll Casting Process, *Acta Metall. Sin.*, 2000, **4**(36), p 391–394 [in Chinese]
14. L. Zhang, J.L. Zhou, X.C. Chen, L. Lan, and N. Zhang, Numerical Simulation of Flow around Square Cylinder Using Different Low-Reynolds number Turbulent Models, *J. Cent. South Univ. Technol.*, 2008, **15**, p 564–568 [in English]